

Synthesis, crystal structure, and chemical stability of the superconductor FeSe_{1-x}E. Pomjakushina,^{1,*} K. Conder,¹ V. Pomjakushin,² M. Bendele,^{3,4} and R. Khasanov⁴¹Laboratory for Developments and Methods, PSI, 5232 Villigen, Switzerland²Laboratory for Neutron Scattering, ETHZ and PSI, 5232 Villigen, Switzerland³Physik-Institut der Universität Zürich, Winterthurerstrasse 190, 8057 Zürich, Switzerland⁴Laboratory for Muon Spin Spectroscopy, PSI, 5232 Villigen, Switzerland

(Received 12 May 2009; revised manuscript received 10 July 2009; published 30 July 2009)

We report on a comparative study of the crystal structure and the magnetic properties of FeSe_{1-x} ($x=0.0-0.15$) superconducting samples by neutron powder-diffraction and magnetization measurements. The samples were synthesized by two different methods: a “low-temperature” one using powders as a starting material at $T \approx 700$ °C and a “high-temperature” method using solid pieces of Fe and Se at $T \approx 1075$ °C. The effect of a starting (nominal) stoichiometry on the phase purity of the obtained samples, the superconducting transition temperature T_c , as well as the chemical stability of FeSe_{1-x} at ambient conditions were investigated. It was found that in the Fe-Se system, a stable phase exhibiting superconductivity at $T_c \approx 8$ K exists in a narrow range of selenium concentration (FeSe_{0.974±0.005}).

DOI: [10.1103/PhysRevB.80.024517](https://doi.org/10.1103/PhysRevB.80.024517)

PACS number(s): 74.70.-b, 74.72.-h, 61.05.fm, 74.25.Ha

I. INTRODUCTION

The discovery of Fe-based superconductors has attracted considerable attention to the pnictides. Superconductivity is detected now in various pnictide families as, e.g., the single-layer ReO_{1-x}F_xFeAs (Re=La, Ce, Pr, Nd, Sm, Gd, Tb, Dy, Ho, and Y),¹⁻⁷ the double-layer MFe₂As₂ (M=Ba, Sr, and Ca),⁸⁻¹² the oxygen free single-layer LiFeAs,¹³⁻¹⁵ etc. The common structural feature of all these materials is the Fe-As layers consisting of a Fe square planar sheet tetrahedrally coordinated by As. Recently, superconductivity with a transition temperature of $T_c \approx 8$ K was discovered in β -FeSe_{1-x} with the PbO structure.¹⁶ This compound also has a Fe square lattice with Fe atoms tetrahedrally coordinated by Se similar to the structure of FeAs layers in the single- and the double-layer pnictides. In this respect FeSe_{1-x}, consisting of the “superconducting” Fe-Se layers only, can be considered as a prototype of the known families of Fe-As-based superconductors and, consequently, is a good model system to study mechanisms leading to the occurrence of superconductivity in this class of materials.

As is stated in the literature, there are two different routes to synthesize superconducting FeSe_{1-x}. The first one uses Se and Fe powders as the starting material and is performed in sealed silica tubes at 400–700 °C.¹⁶ Hereafter we call it the “low-temperature synthesis” (LTS). This method, however, was shown to result in samples with a relatively high amount of impurities. According to Ref. 16, FeSe_{1-x} with $x=0.18$ was found to consist of a superconducting phase and a small amount of elemental selenium, iron oxide, and iron silicide (reaction product with silica ampoule). For a higher average selenium content ($x=0.12$), some amount of hexagonal (NiAs-type) FeSe phase was detected in addition to impurity phases listed above. The superconducting transition temperature was found to be at ≈ 8 K, being independent of the initial Se content. The second procedure proposed in the recent work of McQueen *et al.*¹⁷ starts from Fe pieces and Se shot. The Fe and Se pieces sealed in silica ampoule were first held at 750 °C (3–5 days) then heated up to 1075 °C (3

days) followed by a fast decrease down to 420 °C and quenched. The synthesis was completed by an additional annealing of the sample (sealed in a new ampoule) at 300–500 °C followed by quenching. Superconductivity was found to exist only in a very narrow range of stoichiometry. For FeSe_{0.99} (Fe_{1.01}Se) magnetization measurements showed $T_c \sim 8.5$ K, whereas T_c for FeSe_{0.98} (Fe_{1.02}Se) decreased down to ~ 5 K and went to zero (at least down to 0.6 K) for FeSe_{0.97} (Fe_{1.03}Se).¹⁷ Hereafter, we call this procedure the “high-temperature synthesis” (HTS). In comparison with LTS, the samples prepared by HTS do not contain iron oxide impurities.¹⁷

Surprisingly, the FeSe_{1-x} samples synthesized by LTS and HTS techniques were found to be rather different. Indeed, in LTS samples superconductivity was found in a rather extended range of Se content (at least up to $x=0.18$),^{16,18} while for the HTS superconductivity was detected only in a very narrow region corresponding to $0.01 \leq x \leq 0.025$.¹⁷ In addition, McQueen *et al.*¹⁷ reported that below 300 °C the tetragonal FeSe_{1-x} converts into a hexagonal (NiAs-type) phase, which is not superconducting. Therefore, quenching from temperatures above 300 °C was used for synthesizing HTS samples. On the other hand, no special care for fast cooling of LTS samples needs to be taken.^{16,18} In order to resolve these controversies, we performed comparative studies of the superconducting FeSe_{1-x} samples synthesized by both methods (LTS and HTS) described above. We have improved a method of synthesis using powder starting materials and investigated the effect of stoichiometry on the phase purity of the obtained samples and its superconducting transition temperature. Based on the neutron powder-diffraction (NPD) data, we have revised the Fe-Se concentration phase diagram proposed by Okamoto.¹⁹

II. EXPERIMENTAL DETAILS

AC and DC magnetization (M_{AC}/M_{DC}) measurements were performed using Quantum Design physical property measurement system (PPMS) and magnetic property mea-

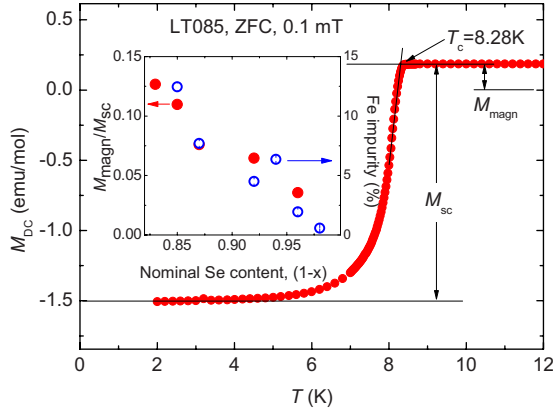


FIG. 1. (Color online) Temperature dependencies of the DC magnetization (M_{DC} , zero-field cooling, 0.1 mT) of LT085 sample. The superconducting transition temperature T_c , the superconducting (M_{SC}), and the magnetic (M_{magn}) responses of the sample are determined as shown in the figure. The inset shows dependencies of M_{magn}/M_{SC} and Fe impurity concentration as a function of the nominal Se content.

surement system (MPMS) at temperatures ranging from 2 to 300 K. The AC field amplitude and the frequency were 0.1 mT and 1000 Hz, respectively. The DC magnetization experiments were performed after zero-field cooling and field cooling the samples at $\mu_0 H = 0.1$ mT. The superconducting transition temperature T_c was determined as an intersection of the linearly extrapolated $M_{AC}(T)[M_{DC}(T)]$ with the $M = \text{const}$ line (see Fig. 1).

NPD experiments were carried out at the SINQ spallation source at the Paul Scherrer Institute (PSI, Switzerland) using the high-resolution diffractometer for thermal neutrons HRPT (Ref. 20) (the neutron wavelengths $\lambda = 1.494$ and 1.155 Å). The refinements of the crystal structure parameters were done using the FULLPROF program,²¹ with the use of its internal tables for neutron-scattering lengths.

III. RESULTS AND DISCUSSION

A. Sample synthesis

Two types of samples using the LTS and the HTS procedures were prepared. Samples of a nominal composition $\text{FeSe}_{0.85}$, $\text{FeSe}_{0.87}$, $\text{FeSe}_{0.92}$, $\text{FeSe}_{0.96}$, $\text{FeSe}_{0.98}$, and FeSe (LT085, LT087, LT092, LT096, LT098, and LT100) were prepared by a solid-state reaction similar to that described in Refs. 16 and 18. The cold-pressed mixtures of Fe and Se powders were sealed in quartz ampoules and then heated up to 700 °C followed by annealing at 400 °C. Powders of Fe and Se of a minimum purity of 99.99% were used as starting materials.

Sample $\text{FeSe}_{0.94}$ (HT094) was synthesized similar to the route of McQueen *et al.*¹⁷—by solid-state reaction using pieces of Fe and Se of a minimum purity of 99.99%. The sample was heated in the sealed quartz ampoule up to 1075 °C followed by annealing at 400 °C. In contrast to McQueen *et al.*,¹⁷ no quenching from high temperatures was made. The sample was cooled down to the room temperature at a rate of 200 °C/h.

Note that for the samples synthesized by both LTS and HTS techniques, all the grindings/pelletizings were performed under helium atmosphere. The samples studied in the present work are listed in Table I.

B. Crystal structure and impurity phases

The crystal structure of the main (superconducting) phase and the concentration of the impurity phases were determined by means of neutron powder diffraction. First, we present the results obtained for the FeSe_{1-x} samples with nominal Se contents $0.85 \leq 1-x \leq 0.98$ (LT085–LT098 and HT094). Room-temperature NPD experiments show that all these samples contain the same tetragonal phase FeSe_{1-x} (space group $P4/nmm$) as a main phase. The refined selenium occupancy (selenium stoichiometry) is about 0.974(2) and is *independent* of the starting composition and the route of the synthesis (LTS; HTS). A typical example of the Rietveld refinement of NPD data is shown in Fig. 2 for the LT098 sample. Impurity phases are hexagonal FeSe (space group $P6_3mmc$) in a quantity of $\sim 1\%$ (molar %) and Fe (space group $Im3m$). Amount of the metallic Fe was found to decrease monotonically with increasing Se content from $\approx 12.5\%$ for $\text{FeSe}_{0.85}$ to $\approx 0.5\%$ for $\text{FeSe}_{0.98}$. Note that for all the samples studied, the presence of any oxides was not detected. The “cleanest” sample is LT098 which contains, in total, less than 2% of the secondary phases and has a nominal composition $\text{FeSe}_{0.98}$; the same as is refined for the main tetragonal phase $\text{FeSe}_{0.975(3)}$. The amount of impurity phases found in the samples, the refined stoichiometry of the main tetragonal phase, and its unit-cell parameters are listed in Table I. It is worth to mention that the samples showing the largest deviation from the average stoichiometry (LT85 and LT100) contain also a relatively large amount of the impurity phases. Therefore, the refined Se occupancy can have some systematic error for these samples. Most NPD measurements were performed with the wavelength $\lambda = 1.494$ Å because it provides the optimal conditions for refining the structure parameters of the main phase (large q range) and determination of the impurity phases (good resolution). To further check for the possible systematic error in the Se occupancy due to its correlation with the atomic displacement parameters, measurements of the most pure sample with yet shorter wavelength $\lambda = 1.155$ Å were performed. The refined Se occupancy was found to be 0.980(3), implying that the systematic error is smaller than 0.005. To better visualize the improvements of the refinement as a function of the Se occupancy ($1-x$), we have calculated the Bragg R factor as a function of $(1-x)$. The structure refinements were performed with all parameters varied except for the fixed value of the occupancy in the range 0.95–1.0. The resulting dependence $R_{\text{Bragg}}(1-x)$ (inset in Fig. 2) nicely shows a minimum around the freely refined value of Se occupancy. Table II shows structure parameters and reliability factors for three samples of FeSe_{1-x} . The sample labeled LT085a that is a degraded on air sample LT085 is presented for comparison and will be discussed in Sec. III D.

We are quite convinced by our structure model because the refinements were really improved if the Se occupancy

TABLE I. Summary of the neutron powder-diffraction and magnetization results for FeSe_{1-x} samples prepared by LTS and HTS methods. Note that the sample LT085a is the air-degraded sample LT085.

Sample name	Nominal composition	T_c (K)	Refined composition phase content (molar %)	Unit-cell parameters of the tetragonal phase (Å)
LT085a	$\text{FeSe}_{0.85}$		$\text{FeSe}_{0.994(11)}$ ($P4/nmm$) $71.75 \pm 1.75\%$ Fe ($Im3m$) $26.23 \pm 0.85\%$ FeSe ($P6_3/mmc$) $2.02 \pm 0.38\%$	$a=3.774$ 13(14) $c=5.521$ 41(31)
LT085	$\text{FeSe}_{0.85}$	8.28	$\text{FeSe}_{0.963(5)}$ ($P4/nmm$) $86.38 \pm 0.98\%$ Fe ($Im3m$) $12.46 \pm 0.33\%$ FeSe ($P6_3/mmc$) $1.16 \pm 0.18\%$	$a=3.773$ 20(4) $c=5.524$ 96(9)
LT087	$\text{FeSe}_{0.87}$	8.34	$\text{FeSe}_{0.979(4)}$ ($P4/nmm$) $91.53 \pm 0.91\%$ Fe ($Im3m$) $7.70 \pm 0.23\%$ FeSe ($P6_3/mmc$) $0.77 \pm 0.14\%$	$a=3.772$ 80(4) $c=5.523$ 03(8)
LT092	$\text{FeSe}_{0.92}$	8.44	$\text{FeSe}_{0.976(4)}$ ($P4/nmm$) $94.50 \pm 0.89\%$ Fe ($Im3m$) $4.50 \pm 0.21\%$ FeSe ($P6_3/mmc$) $1.00 \pm 0.13\%$	$a=3.773$ 35(4) $c=5.523$ 68(8)
HT094	$\text{FeSe}_{0.94}$	8.21	$\text{FeSe}_{0.977(3)}$ ($P4/nmm$) $92.91 \pm 0.70\%$ Fe ($Im3m$) $6.36 \pm 0.16\%$ FeSe ($P6_3/mmc$) $0.73 \pm 0.09\%$	$a=3.772$ 94(4) $c=5.524$ 21(7)
LT096	$\text{FeSe}_{0.96}$	8.43	$\text{FeSe}_{0.978(4)}$ ($P4/nmm$) $96.02 \pm 1.07\%$ Fe ($Im3m$) $1.94 \pm 0.23\%$ FeSe ($P6_3/mmc$) $2.04 \pm 0.19\%$	$a=3.773$ 38(5) $c=5.524$ 15(11)
LT098	$\text{FeSe}_{0.98}$	8.21	$\text{FeSe}_{0.975(3)}$ ($P4/nmm$) $98.31 \pm 0.59\%$ Fe ($Im3m$) $0.57 \pm 0.05\%$ FeSe ($P6_3/mmc$) $1.12 \pm 0.08\%$	$a=3.773$ 81(2) $c=5.523$ 30(5)
LT100	FeSe_1	~ 8	$\text{FeSe}_{0.968(3)}$ ($P4/nmm$) $83.03 \pm 0.61\%$ Fe ($Im3m$) $0.46 \pm 0.05\%$ Fe_7Se_8 ($P3_121$) $16.51 \pm 0.28\%$	$a=3.773$ 53(4) $c=5.523$ 82(7)

was released and the refined composition exactly corresponded to the starting composition that gave the cleanest final sample as we explained above. However, there is an alternative structure that also would correspond to Se deficiency of the initial composition observed in the isostructural $\text{Fe}_{1.125}\text{Te}$,²² where the extra Fe atoms are located at the interstitial sites ($2c$) ($1/4, 1/4, z$), $z \approx 0.5$. We have made the refinements in this model for the best sample LT098 and found that this model does not fit to our experimental data at all. The above described procedure used to obtain the plot in the inset of Fig. 2 shows that the R factor $R_{\text{Bragg}}(x_{\text{Fe}})$ steadily increases with the increase in the Fe occupancy x_{Fe} from 3.99 for $x_{\text{Fe}}=0.01$ to more than 4.4 for $x_{\text{Fe}} > 0.03$.

The results of the structural analysis were further confirmed by magnetic-susceptibility measurements. As follows from Table I, all FeS_{1-x} samples ($0 < x \leq 0.15$) have almost the same transition temperatures ($T_c \sim 8.2\text{--}8.4$ K) and, consequently, very similar doping (concentration of charge carriers). In addition, the paramagnetic offset (M_{magn}) seen at $T > T_c$ was found to decrease with increasing Se content just following the dependence of Fe impurity phase as the function of the nominal Se content $1-x$ (see the inset in Fig. 1). Note that in Ref. 23 the observation of the paramagnetic offset at $T > T_c$ as well as the static magnetic contribution seen in zero-field muon-spin rotation experiments were attributed to the presence of Fe impurities.

By increasing the Fe:Se ratio up to 1:1, the situation was drastically changed. The Rietveld refinement of NPD data on FeSe (LT100) sample reveals that the main tetragonal phase content is substantially decreased down to $\approx 83.03\%$. The content and the composition of the impurity phases were also changed: only 0.46% of Fe and, instead of a hexagonal NiAs-type phase $\approx 16.51\%$ of the trigonal Fe_7Se_8 (space group $P3_121$) was detected. Magnetization experiments also show a substantial decrease in the superconducting fraction, which was found to be of about 10% at $T=3$ K.

Studies of the crystal structure of the main phase as a function of temperature were performed on the sample LT085 in the temperature range 20–300 K on both cooling and heating. Figure 3 shows the lattice constants a and b and the unit-cell volume as a function of temperature. At temperature $T=100$ K, there is a transition from the tetragonal to orthorhombic structure on cooling similar as observed in Ref. 18. The low-temperature structure is well refined in the space group $Cmma$. The building block of the crystal structure is SeTe_4 square pyramid with Se atom in the apex. In the high-temperature phase the pyramid is regular, whereas in the orthorhombic phase the neighboring Fe-Fe-Fe bond angles become different as shown in Fig. 4. The Se-Fe bond length amounts to 2.386(2) Å at low temperature and it is not changed at the transition. Neither temperature hysteresis nor the unit-cell volume jump was observed indicating that

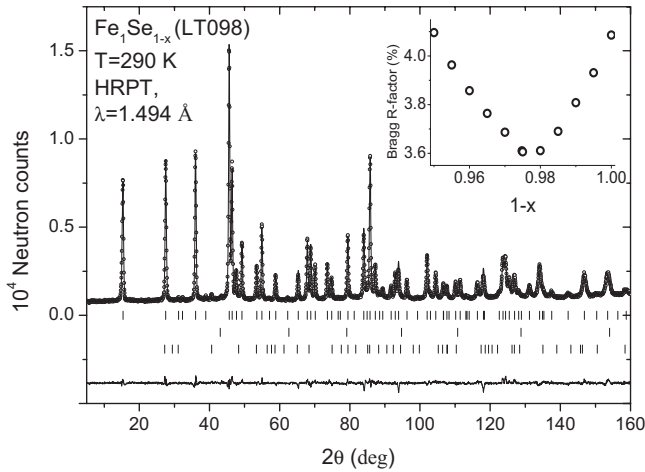


FIG. 2. The Rietveld refinement pattern and difference plot of the neutron-diffraction data for the sample Fe_{1-x}Se (LT098) at $T = 290$ K measured at HRPT with the wavelength $\lambda = 1.494$ Å. The rows of ticks show the Bragg-peak positions for the main phase and two impurity phases. The main tetragonal phase corresponds to 0.975(3) Se content. The inset shows Bragg R factor plotted versus Se occupancy. See text for details.

the transition is of the second-order type. The transition temperature in our sample $\text{FeSe}_{0.963(5)}$ (100 K) is different from the one reported for $\text{FeSe}_{0.91}$ (70 K) (Ref. 18) that might be related to the different Se stoichiometry. However, as described above our synthesis techniques always produce the main tetragonal phase with approximately the same concentration with the average value of about $x = 0.974$.

C. Phase diagram

In this section, stoichiometry of the main phase and the phase composition of the studied samples are discussed

TABLE II. Structural parameters of the FeSe_{1-x} main phase of the “cleanest” sample LT098, the sample with largest impurity admixture LT085, and the degraded sample LT085a (discussed in Sec. III D) at 290 K. Space group $P4/nmm$ (no. 129), origin choice 2. Fe in (2b) position (1/4,3/4,1/2); Se in (2c) position (1/4,1/4,z) The atomic displacement parameters for Fe and Se were constrained to be the same. The Bragg R factor is given for the main phase; the other reliability factors are given for the whole refinement.

	LT098	LT085	LT085a
$a(\text{Å})$	3.77381(2)	3.77320(4)	3.77413(14)
$c(\text{Å})$	5.52330(5)	5.52496(9)	5.52141(31)
c/a	1.46359	1.46426	1.46296
$z\text{-Se}$	0.23268(14)	0.2331(3)	0.2334(8)
occupancy	0.975(2)	0.963(5)	0.99(1)
$B(\text{Å}^2)$	1.01(1)	1.09(2)	1.54(5)
R_{Bragg}	3.61	5.83	8.35
χ^2	2.63	1.61	1.54
R_{wp}	4.21	3.83	4.53
R_{exp}	2.60	3.02	3.65

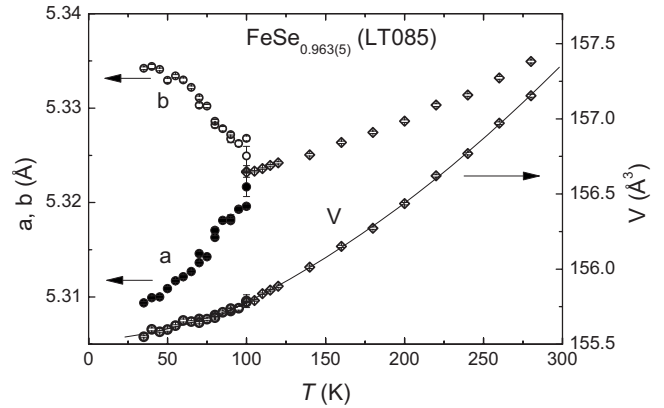


FIG. 3. a, b unit-cell parameters and unit-cell volume V as a function of temperature. In the tetragonal phase, the lattice constant is multiplied by $\sqrt{2}$.

based on the existing Fe-Se binary phase diagrams elaborated by Okamoto¹⁹ and McQueen *et al.*¹⁷ Figure 5 shows a combined phase diagram based on the previously published data.^{17,19} Lines correspond to the part of the binary phase diagram reported in Ref 19. The stripe centered at around 49.5 at. % of Se corresponds to a range of existence of tetragonal above 300 °C and hexagonal FeSe_{1-x} (NiAs-type) below 300 °C as proposed in Ref. 17. The circles correspond to the samples with different nominal Se content studied in this work. The refined selenium stoichiometry ($1-x$) of the main superconducting phase for all the investigated samples are plotted in the inset. The existence range of the nonstoichiometric FeSe_{1-x} as proposed in Ref. 17 is also shown. The average stoichiometry of the superconducting phase was determined to be $\text{FeSe}_{0.974(2)}$ (the error bar represents the statistical error). The average Se concentration is represented by the vertical line in the inset and it is very close to that for the most pure sample LT098 [$\text{FeSe}_{0.975(3)}$], which is shown by the solid point in the inset.

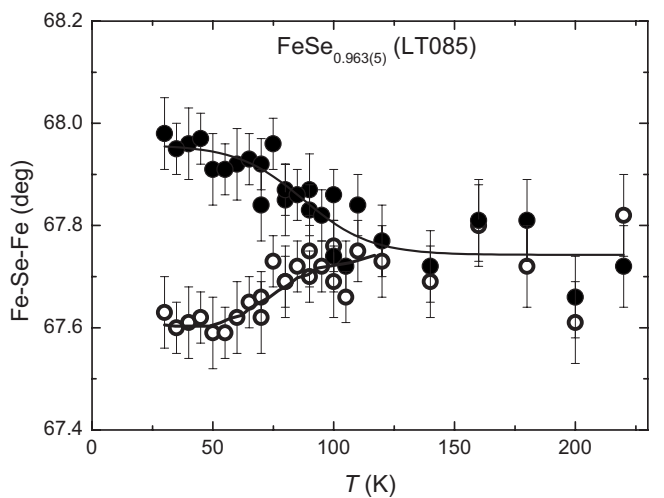


FIG. 4. Fe-Se-Fe bond angles as a function of temperature in $\text{FeSe}_{0.963(5)}$. The refinements of the diffraction data were made assuming low-symmetry phase (space group $Cmma$). The high-temperature crystal structure is tetragonal and both Fe-Se-Fe angles would be the same by symmetry in $P4/nmm$ group.

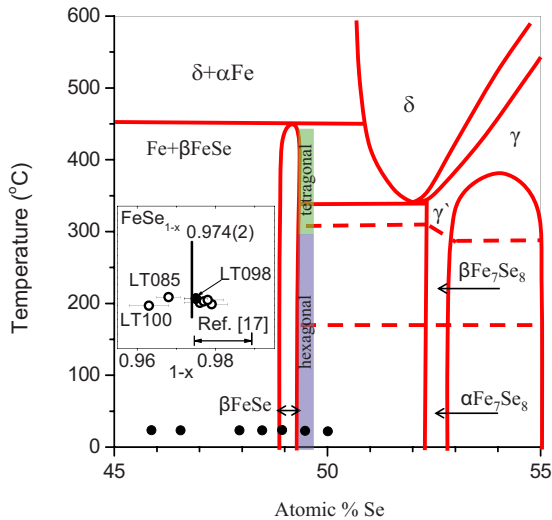


FIG. 5. (Color online) The Fe-Se phase diagram after Okamoto (Ref. 19) (lines) and McQueen *et al.* (Ref. 17) (vertical colored stripe). The black circles correspond to the nominal composition of the samples studied in the present work. In the inset, the refined selenium stoichiometry ($1-x$) of the main superconducting phase found in all the investigated samples is plotted together with the range of the existence of nonstoichiometric FeSe_{1-x} as proposed in Ref. 17. See text for details.

From the data presented in Fig. 5, the following important statements emerge: (i) the stability field of the superconducting tetragonal β -FeSe phase as proposed in Ref. 17 does not overlap with that reported in Ref. 19. According to Ref. 17, the tetragonal phase exists only at high temperatures, but it is transformed to the hexagonal one below 300 °C; (ii) all the samples studied in our work contain the superconducting tetragonal phase as the main phase with almost the same average stoichiometry ($\text{FeSe}_{0.974(2)}$) (see the inset in Fig. 5 and Table I) and display the same $T_c \approx 8$ K. This is in disagreement with the results of Ref. 17 because the compounds with the stoichiometries shown by points in the inset of Fig. 5 would have to display lower (~ 5 K) or even vanishing T_c ; (iii) the present work demonstrates that there is no need for quenching from high temperatures (300–450 °C) in order to get a stable at room temperature and pure tetragonal phase. According to our NPD studies, the $\text{FeSe}_{0.98}$ (LT098) sample contains, in total, less than 2% of impurity phases. Consequently, our data do not prove an existence of tetragonal-hexagonal phase transition on cooling at ~ 300 °C as proposed in Ref. 17; (iv) our data suggest very narrow range or even strictly defined stoichiometry of the superconducting tetragonal FeSe_{1-x} phase. It looks that the composition of this phase is located between the fields proposed in both Refs. 17 and 19. An additional confirmation of the correct locus of the tetragonal phase on the phase diagram comes from an investigation of a phase composition of the LT100 sample (nominally $\text{FeSe}_{1.00}$). According to the phase diagram,¹⁹ this sample should be in the two phase region ($\beta\text{FeSe}-\alpha\text{Fe}_7\text{Se}_8$) at room temperature. Using a lever rule $\sim 18\%$ Fe_7Se_8 would be expected being in a good agreement with 16.5% as found from NPD data (see Table I).

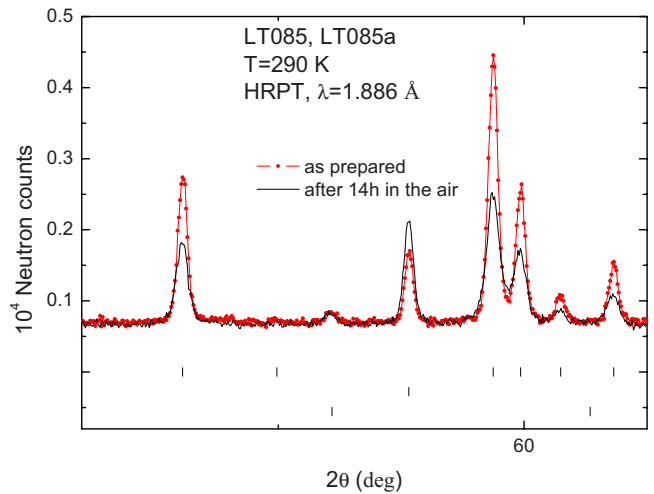


FIG. 6. (Color online) Neutron powder-diffraction pattern of LT085 and LT085a samples at $T=290$ K measured at HRPT with the wavelength $\lambda=1.886$ Å. The red dotted curve corresponds to the as-prepared sample (LT085). The solid black curve was obtained after exposing the sample for 14 h in the air (LT085a). See text for details.

D. Chemical stability of FeSe

In order to study the chemical stability of FeSe samples, the LT085 sample was powderized and stored in air for 14 h (LT085a) and then measured by means of NPD. In Fig. 6, the Rietveld refinement of a neutron-diffraction pattern of LT085a sample (solid line) together with as-prepared LT085 sample (dotted curve) taken at room temperature are presented. The sample underwent drastic changes after exposing in air. Volume fraction of the main tetragonal phase was decreased from 93% down to 84%, whereas the quantity of Fe increases from 6% up to 13%, at the same time the increase of the of the hexagonal phase content was not so pronounced. The diffraction peaks of the main phase of LT085a sample show severe broadening and, at the same time, the atomic displacement parameters (Debye-Waller factor) increase by 1.5 times, thus, implying the presence of both large scale defects (e.g., dislocations or the presence of new-phase particles) and point defects (e.g., vacancies).²⁴ Additionally, it was found that the stoichiometry of the main phase becomes almost 1:1 (Fe:Se). The integral counting rates (scale factors) further reveal that about 20–30 % of the main phase was lost (most probably, it became amorphous).

In order to figure out the reason of FeSe_{1-x} degradation, additional experiments were performed. The $\text{FeSe}_{0.98}$ (LT098) sample was divided in three parts. Each of them was further powderized and exposed in pure helium, oxygen, and air atmosphere. Figure 7 shows $M_{DC}(T)$ curves obtained for the different parts of the sample. It is obvious that both air and oxygen lead to a dramatic degradation of the superconducting properties. Indeed, the superconducting volume fraction decreases by more than a factor of 5, while the T_c onset shifts to the lower temperature. At the same time, the superconducting transition becomes very broad—the magnetization decreases continuously from T_c down to 2 K. We suppose, therefore, that by exposing FeSe sample in the air or in

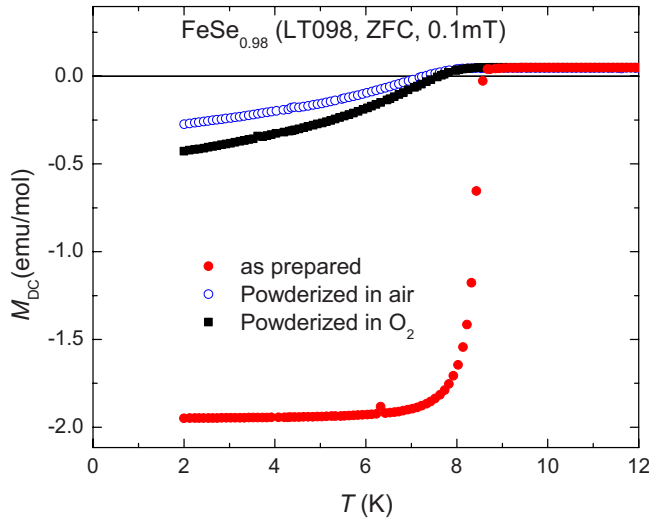


FIG. 7. (Color online) Temperature dependencies of the DC magnetization (M_{DC} , zero-field cooling, 0.1 mT) of LT098 sample. The experimental data correspond to the sample: (●) as prepared; (○) powderized/exposed in the air; and (■) powderized/exposed in pure oxygen.

the oxygen atmosphere it decomposes by oxidizing (most probably forming SeO_2).

IV. CONCLUSIONS

A comparative study of the crystal structure and the magnetic properties of the superconductor FeSe_{1-x} synthesized at lower temperatures from powders and at higher temperatures from pieces of metal was performed. The effect of a starting (nominal) stoichiometry on a phase purity of the obtained samples and their superconducting transition temperatures T_c

was studied. On the base of our neutron powder-diffraction data, we have revised the Fe-Se concentration phase diagram proposed by Okamoto.¹⁹ In particular, we have found that in the Fe-Se system a stable phase exhibiting superconductivity at $T_c \sim 8$ K exists in the narrow range of selenium concentration ($\text{FeSe}_{0.974 \pm 0.005}$).

As revealed by the NPD study, at $T \sim 100$ K FeSe_{1-x} undergoes a second-order structural phase transition from a tetragonal phase (space group $P4/nmm$) to an orthorhombic (space group $Cmma$) on cooling. Fe-Se-Fe bond angles in the FeSe_4 pyramids become different in low-temperature phase, whereas the Fe-Se bond lengths are not changed at the transition.

The chemical stability of FeSe samples exposed in air and in pure oxygen atmosphere was studied. It was found that after exposing in air the structure gets many defects, as revealed by NPD diffraction peaks broadening and the large increase in the atomic displacement parameters. The amount of both impurity phases increases about two times reaching 26% for metallic iron and 2% for the hexagonal FeSe. This leads to a dramatic degradation of the superconducting properties, which was proved by magnetization measurements.

ACKNOWLEDGMENTS

The authors are grateful to Hugo Keller for helpful discussions. This study was partly performed at Swiss neutron spallation SINQ of Paul Scherrer Institute PSI (Villigen, PSI). We acknowledge the allocation of the beam time at the HRPT diffractometer of the Laboratory for Neutron Scattering (ETHZ & PSI, Switzerland). The authors thank the NCCR MaNEP project and the Swiss National Science Foundation for the support of this study.

*ekaterina.pomjakushina@psi.ch

- ¹Y. Kamihara, T. Watanabe, M. Hirano, and H. Hosono, *J. Am. Chem. Soc.* **130**, 3296 (2008).
- ²C. Wang, L. Li, S. Chi, Z. Zhu, Z. Ren, Y. Li, Y. Wang, X. Lin, Y. Luo, S. Jiang, X. Xu, G. Cao, and Z. Xu, *EPL* **83**, 67006 (2008).
- ³Z.-A. Ren *et al.*, *EPL* **83**, 17002 (2008).
- ⁴A. S. Sefat, M. A. McGuire, B. C. Sales, R. Jin, J. Y. Howe, and D. Mandrus, *Phys. Rev. B* **77**, 174503 (2008).
- ⁵G. F. Chen, Z. Li, D. Wu, G. Li, W. Z. Hu, J. Dong, P. Zheng, J. L. Luo, and N. L. Wang, *Phys. Rev. Lett.* **100**, 247002 (2008).
- ⁶H. Wen, G. Mu, L. Fang, H. Yang, and X. Zhu, *EPL* **82**, 17009 (2008).
- ⁷J. Yang, X. Shen, W. Lu, W. Yi, Z. Li, Z. Ren, G. Che, X. Dong, L. Sun, F. Zhou, and Z. Zhao, *New J. Phys.* **11**, 025005 (2009).
- ⁸M. Rotter, M. Tegel, D. Johrendt, I. Schellenberg, W. Hermes, and R. Pottgen, *Phys. Rev. B* **78**, 020503(R) (2008).
- ⁹M. Rotter, M. Tegel, and D. Johrendt, *Phys. Rev. Lett.* **101**, 107006 (2008).
- ¹⁰G. F. Chen, Z. Li, G. Li, W. Z. Hu, J. Dong, X. D. Zhang, P.

Zheng, N. L. Wang, and J. L. Luo, *Chin. Phys. Lett.* **25**, 3403 (2008).

- ¹¹N. Ni, S. Nandi, A. Kreyssig, A. I. Goldman, E. D. Mun, S. L. Bud'ko, and P. C. Canfield, *Phys. Rev. B* **78**, 014523 (2008).
- ¹²M. S. Torikachvili, S. L. Bud'ko, N. Ni, and P. C. Canfield, *Phys. Rev. Lett.* **101**, 057006 (2008).
- ¹³G. Wu, H. Chen, Y. L. Xie, Y. J. Yan, T. Wu, R. H. Liu, X. F. Wang, D. F. Fang, J. J. Ying, and X. H. Chen, *Phys. Rev. B* **78**, 092503 (2008).
- ¹⁴M. J. Pitcher, D. R. Parker, P. Adamson, S. J. C. Herkelrath, A. T. Boothroyd, M. R. Ibberson, M. Brunelli, and S. J. Clarke, *Chem. Commun. (Cambridge)* **2008**, 5918.
- ¹⁵J. H. Tapp, Z. Tang, B. Lv, K. Sasmal, B. Lorenz, P. C. W. Chu, and A. M. Guloy, *Phys. Rev. B* **78**, 060505(R) (2008).
- ¹⁶F.-C. Hsu, J.-Y. Luo, K.-W. Yeh, T.-K. Chen, T.-W. Huang, P. M. Wu, Y.-C. Lee, Y.-L. Huang, Y.-Y. Chu, D.-C. Yan, and M.-K. Wu, *Proc. Natl. Acad. Sci. U.S.A.* **105**, 14262 (2008).
- ¹⁷T. M. McQueen, Q. Huang, V. Ksenofontov, C. Felser, Q. Xu, H. Zandbergen, Y. S. Hor, J. Allred, A. J. Williams, D. Qu, J. Checkelsky, N. P. Ong, and R. J. Cava, *Phys. Rev. B* **79**, 014522

- (2009).
- ¹⁸S. Margadonna, Y. Takabayashi, M. T. McDonald, K. Kasperkiewicz, Y. Mizuguchi, Y. Takano, A. N. Fitch, E. Suard, and K. Prassides, *Chem. Commun. (Cambridge)* **2008**, 5607.
- ¹⁹H. Okamoto, *J. Phase Equilib.* **12**, 383 (1991).
- ²⁰P. Fischer, G. Frey, M. Koch, M. Könnecke, V. Pomjakushin, J. Schefer, R. Thut, N. Schlumpf, R. Bürge, U. Greuter, S. Bondt, and E. Berruyer, *Physica B* **276-278**, 146 (2000).
- ²¹J. Rodríguez-Carvajal, *Physica B* **192**, 55 (1993).
- ²²D. Fruchart, P. Convert, P. Wolfers, R. Madar, J. P. Senateur, and R. Fruchart, *Mater. Res. Bull.* **10**, 169 (1975).
- ²³R. Khasanov, K. Conder, E. Pomjakushina, A. Amato, C. Baines, Z. Bukowski, J. Karpinski, S. Katrych, H.-H. Klauss, H. Luetkens, A. Shengelaya, and N. D. Zhigadlo, *Phys. Rev. B* **78**, 220510(R) (2008).
- ²⁴M. A. Krivoglaz, *X-Ray and Neutron Diffraction in Nonideal Crystals* (Springer-Verlag, Berlin, 1996).